analytical chemistry

Article

Endoplasmic Reticulum-Targeted Ratiometric NHC-Borane Probe for Two-Photon Microscopic Imaging of Hypochlorous Acid

Yenleng Pak, Sang Jun Park, Gyeongok Song, Yubin Yim, Hyuk Kang, Hwan Myung Kim, Jean Bouffard, and Juyoung Yoon

Anal. Chem., **Just Accepted Manuscript** • DOI: 10.1021/acs.analchem.8b03565 • Publication Date (Web): 10 Oct 2018

ACS Publications

is published by the American Chemical Society. 1155 Sixteenth Street N.W., Washington, DC 20036

Endoplasmic Reticulum-Targeted Ratiometric NHC-Borane Probe for Two-Photon Microscopic Imaging of Hypochlorous Acid

Yen Leng Pak[‡a], Sang Jun Park[‡b], Gyeongok Song[c], Yubin Yim[a], Hyuk Kang[c], Hwan Myung Kim*[b,c], Jean Bouffard*[a], and Juyoung Yoon*[a]

[a]Department of Chemistry and Nano Science, Ewha Womans University, Seoul 120-75003760, Korea

[b]Department of Energy Systems Research, Ajou University, Suwon, Gyeonggi-do 443-749, Korea

[c]Department of Chemistry, Ajou University, Suwon, Gyeonggi-do 443-749, Korea.

ABSTRACT: The naphthoimidazolium borane **4** is shown to be a selective probe for HOCl over other reactive oxygen species. Unlike other boronate-ROS fluorogenic probes that are oxidized by HOCl through a nucleophilic borono-Dakin oxidation mechanism, probe **4** is distinguished by its electrophilic oxidation mechanism involving B–H bond cleavage. Two-photon microscopy experiments in living cells and tissues with the probe **4** demonstrate the monitoring of endogenous HOCl generation and changes in HOCl concentrations generated in the endoplasmic reticulum during oxidative stress situations.

In all aerobic living organisms, reactive oxygen species (ROS) are continuously produced, transformed, and consumed. They are generated endogenously and actively participate as metabolite agents in signaling pathways to support the normal function of cells.[1,2] Oxidative stress, which results from an unbalance between the levels of ROS and antioxidants inside the cell, causes cell damage and contributes to the aging process.[3,4] Their short lifetimes and low concentrations make their *in vivo* measurement and the study of their biological roles more challenging. Among other methods, fluorescence imaging probes have emerged as powerful measurement tools to visualize the variation and distribution of these species, with a popularity owed to their real-time monitoring capabilities, high sensitivity, and non-invasive characteristics.[5-20]

Notwithstanding earlier advances, there is an unmet need for analytical methods capable of measuring the concentrations of ROS and other analytes in specifically targeted organelles. For fluorescence imaging, this requires probes to be transported into the specific organelle of a living system, and to be inactive before their localization in that organelle.[21-24] The largest organelle, the endoplasmic reticulum (ER) is responsible for essential metabolic functions in cells.[25,26] The unique oxidizing conditions maintained within the ER, in particular, are critical for its role in protein folding and disulfide bond formation.[27,28] The specific role of the different ER ROS generated during oxidative protein folding processes and other signaling mechanisms remains ambiguous, due to the lack of ER-specific probes for these species.[29-31] Thus, the preparation of specific probes for ROS located in the ER is of great importance.

Aryl boronic acids and their esters have been broadly used in the design of fluorescent sensors to detect and screen intracellular ROS,[32,33] such as hydrogen peroxide,[34-41] hypochlorite (OCl^-)[42,43] and peroxynitrite ($ONOO^-$)[44-47] Their design relies on the well-known ROS-mediated oxidation of boronate derivatives to phenols that proceed through a borono-Dakin reaction mechanism.

Earlier in 2018, we have reported the first use of an N-heterocyclic carbene borane (NHC-borane) as a ROS probe specific for HOCl.[48] The reported probe **5** was shown to react with HOCl through an electrophilic mechanism that proceeds with a formal hydride abstraction at the borane center, in contrast with the nucleophilic mechanism for the reaction of OCl^- with boronic acids their esters. After oxidative hydrolysis by HOCl, electrostatic repulsion between the resulting imidazolium salts disfavors the formation of colloidal fluorophore aggregates and pyrene excimers.

Herein, we report the design and application of a second NHC-borane-based fluorogenic probe **4** for the specific detection of HOCl. Unlike its predecessor, its turn-on luminescence signal does not rely on polarity and aggregation effects. Instead, oxidative hydrolysis of the B–H bonds of **4** occurs in the presence of HOCl to yield the emissive naphthoimidazolium derivative **3**. The latter was chosen on the basis of our earlier work, which showed in 2015 that 1,3-dimethyl-1,3-dihydro-2*H*-naphtho[2,3-*d*]imidazole-2-thione (**6**) is oxidized at sulfur by HOCl to also give **3**.[49] The resulting increased emission at 450 nm established the suitability of the latter as a fluorescence reporter. The new probe **4** is highly selective for HOCl, overcomes the aggregation effects of the previously reported **5**, and is suitable for the two-photon microscopic (TPM) imaging of endogenous HOCl generation in living cells and tissues. Moreover, **4** exhibits outstanding ER-targetability comparable to that of commercial ER trackers, enabling the monitoring by TPM of HOCl production within ER in cells under ER stress conditions.

Scheme 1. a) Synthesis of 4 and b) proposed mechanism for the reaction of 4 with HOCl.

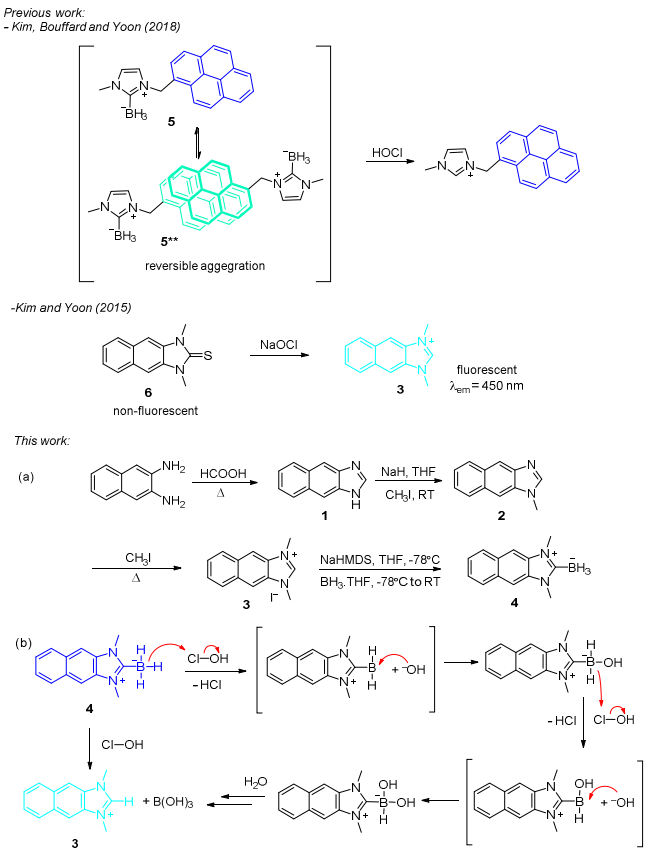

EXPERIMENTAL SECTION

Materials and Chemicals. Solvents and chemicals used for synthesis and purification were obtained from commercial suppliers and used without further purification. Synthetic operations that required an inert atmosphere (where noted) were conducted under a nitrogen atmosphere. ^{1}H, ^{11}B and ^{13}C NMR spectra were obtained with 300 MHz and 500 MHz Bruker Avance spectrometers. Chemical shifts are reported as δ in units of parts per million (ppm) vs. Si $(CH_4)_4$ (^{1}H, ^{13}C) or $BF_3{\cdot}OEt_2$ (^{11}B), referenced to the residual solvent. Splitting patterns are represented as s (singlet), d (doublet), t (triplet), q (quartet), m (multiplet), and br (broad). Electrospray ionization (ESI) mass spectra were collected on an Agilent G6550A Q-TOF mass spectrometer at the Seoul branch of the Korean Basic Science Institute. A Jeol JMS 700 high resolution mass spectrometer was used to acquire FAB mass spectra at the Korea Basic Science Institute (Daegu). UV absorption spectra were collected on a UVIKON 933 double-beam UV-vis spectrometer, and a RF-5301/PC spectrofluorophotometer (Shimadzu) was used to record the fluorescence emission spectra.

Synthesis of (1,3-dimethyl-1*H*-naphtho[2,3-*d*]imidazolium-2-yl)trihydroborate(4). Sodium bis(trimethylsilyl)amide (1 M in dry THF, 0.51 mL, 2.79 mmol) was added drop-wise to a suspension of **3**[49] (0.5 g, 2.53 mmol) in anhydrous THF (10 mL) at -78˚C. The resulting mixture was stirred for 1h at -78˚C. Next, $BH_3{\cdot}$THF (1 M in THF, 0.24 mL, 2.79 mmol) was added to the mixture. The resulting solution was stirred overnight and slowly warmed to ambient temperature. The crude mixture was purified by flash chromatography (SiO_2, CH_2Cl_2) after evaporation of the volatiles to yield **4** as a white solid (0.12 g, 23 %). ^{1}H NMR (300 MHz, $CDCl_3$) δ (ppm): 8.05-8.00 (m, 2H), 7.83 (m, 2H), 7.58-7.52 (m, 2H), 4.07 (s, 6H), 1.74-1.16 (q, $J_{B\text{-}H}$ = 90 Hz, 3H). ^{13}C NMR ($CDCl_3$, 62.5 MHz): δ 133.3, 130.7, 128.3, 125.8, 107.3, 32.5 (C-B not seen). ^{11}B NMR (160.4 MHz, $CDCl_3$): δ -36.9 (q, $J_{B\text{-}H}$ = 90 Hz). FAB-MS calcd. for $C_{13}H_{14}BN_2$ $[M\text{-}H]^+$: 209.1245; found 209.1252.

Fluorescence Studies. A 1 mM stock solution of **4** was prepared in acetonitrile (CH_3CN). To prepare a final concentration of 10 μM, the stock solution of probe **4** was diluted with PBS (10 mM, pH = 7.4, 10% CH_3CN), and then an appropriate aliquot of ROS or RNS solutions was added before transfer to quartz cuvettes for spectroscopic measurements. Samples were excited at 326 nm, with excitation and emission slit widths of 3.0 nm for all fluorescence experiments.

Generation of ROS or RNS. H_2O_2, sodium hypochlorite (NaOCl), and *tert*-Butyl hydroperoxide (^{t}BuOOH) were obtained by dilution from commercial aqueous solutions. Hydroperoxyl radicals (ROO•) were prepared from 2,2'-azobis(2-amidinopropane) dihydrochloride.[50] Nitric oxide radical (•NO) was generated from SNP (sodium nitroferricyanide (III) dihydrate). The hydroxyl radical (•OH) was produced from the reaction between iron (II) chloride (200 μM) and H_2O_2 (400 μM). $ONOO^-$ was prepared following reported procedures, and its concentration was determined by spectrophotometry (ε =1670 $M^{-1}{\cdot}cm^{-1}$ at 302 nm).[51]

RESULTS AND DISCUSSION

The overall synthetic route of **4** is presented in Scheme 1a. Specifically, the reaction of the naphthoimidazolium precursor **3** with a borane source (BH_3 in THF) in the presence of a non-nucleophilic base (NaHMDS) afforded **4** in 23% yield.

The spectral responses of **4** to ROS were examined by using UV-Vis absorption and fluorescence emission spectroscopy in aqueous buffered solution (10 mM PBS containing 10 % of CH_3CN). As presented in Figure S1a, the absorbance band for **4** is centered at ca. 322 nm. This band is not shifted but becomes broader with hypochromism upon the addition of 100 μM OCl^-. The probe itself emits violet-blue light (Φ = 0.42) at 361 nm when excited at 326 nm. When the aqueous solution of **4** was treated with different concentrations of OCl^- (0-100 μM), the emission peak at 361 nm disappeared, and a cyan fluorescence band at 450 nm grew concomitantly (Figure 1). The UV and emission spectra of **4** after reaction with OCl^- matched that of **3** (Φ = 0.29) (Figure S1).

To explain the difference in the absorption and emission spectra of **3** and **4**, time-dependent density functional theory (TD-DFT) calculations were performed (Table S1 and Figure S2). Vertical excitation energies for **3** and **4** were calculated to account for the different absorption maxima in their UV-visible spectra. Naphthoimidazolium salt **3** shows longer transition wavelength and lower oscillator strength than probe **4**, which agrees well with its longer absorption maximum and lower absorbance in solution. Similarly, **3** shows a longer emission maximum than **4**. Both **3** and **4** show higher electron density of LUMO on the imidazole ring than that of HOMO, and the excitation can be characterized as a partial charge transfer excitation from the naphthalene to the imidazole moiety (Figure S2). Hence, the more apparent charge transfer character of **3** explains its longer absorption and emission wavelengths in solution than those of **4**.

The changes in the ratio between the intensity of the two emission bands (450 nm for **3** and 361 nm for **4**) during the addition of hypochlorite were recorded (Figure S3). The F_{450}/F_{361} ratio increased from 0.05 to 23.41 upon treatment of a solution of **4** with 100 μM OCl^-, representing ca. 470-fold ratiometric signal response. The calculated detection limit of **4** for OCl^- was found to be 3.6 μM (Figure S4). The fluorescence ratios for **4** before or after the addition of OCl^- remained stable in the 2-10 pH range (Figure S5). The large changes in ratiometric response were deemed sufficient to apply **4** to the monitoring of hypochlorite concentrations under physiological conditions. Time courses experiments were performed on **4** by recording the fluorescence intensity at 450 nm for 60 min (Figure S6). The emission signal increased immediately, and reached a maximum fluorescence at 450 nm within 1 min after addition of either 30 μM or 100 μM OCl^-. The fluorescence intensities remained largely unchanged over extended monitoring time (up to 60 min). The stability of the probe and its response to OCl^- are particularly suitable to monitor the generation of OCl^- in living systems.

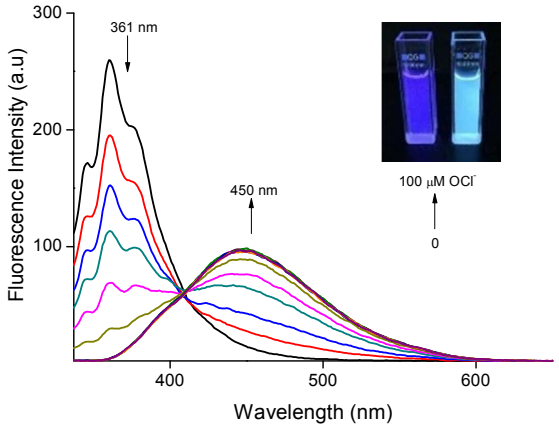

Figure 1. Fluorescence spectra of **4** (10 μM) upon addition of OCl^- (0-100 μM) in PBS/CH_3CN (v/v, 9/1, 10 mM PBS, pH 7.4). Inset: Image of a **4** solution before (left) and after (right) addition of OCl^- under UV irradiation.

Selectivity is a major issue in molecular sensing. . The selectivity of 4 toward biological relevant metal ions and ROS/RNS species including OCl-, H2O2, •OH, tBuOOH, •NO, ONOO-, ROO•, O2•-, and 1O2 were examined. As expected from earlier experiments with NHC-boranes,48 4 is highly selective to OCl- over others ROS/RNS and metal ions shown in Figure 2 Only OCl^- elicited a ratiometric signal response (F_{450}/F_{361}), and other analytes displayed no interference.

Stimulated by the above promising outcomes in vitro, the aptitude of **4** for sensing endogenous OCl^- in a ratiometric manner by two-photon fluorescence microscopy was investigated. Probe **4** itself was first found to have low cytotoxicity to living HeLa cells through standard MTT assays (Figure S8). The fluorescence intensity of Raw 264.7 cells incubated with **4** (10 μM) showed high photostability during 1 h irradiation at 720 nm wavelength (Figure S9).

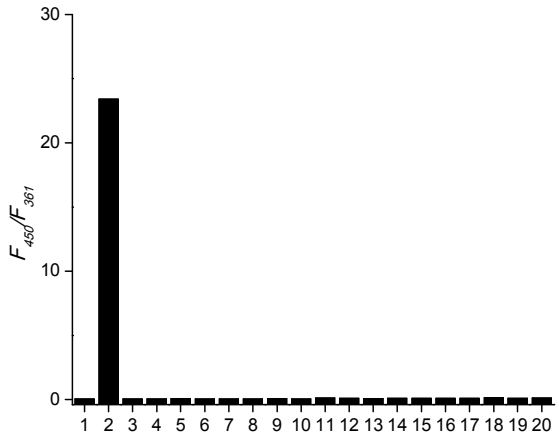

Figure 2. Fluorescence ratio (F_{450}/F_{361}) of **4** (10 μM) in PBS/MeCN (v/v, 9/1) toward 100 μM of different analytes: 1) Blank, 2) OCl^-, 3) H_2O_2, 4) •OH, 5) ^{t}BuOOH, 6) •NO, 7) $ONOO^-$, 8) ROO•, 9) $O_2^{\bullet-}$, 10) $^1O_2$, 11) Na^+, 12) K^+, 13) Ca^{2+}, 14) Mg^{2+}, 15) Zn^{2+}, 16) Al^{3+}, 17) Cu^{2+}, 18) Fe^{2+}, 19) Fe^{3+} and 20) Mn^{2+}.

According to our previous report,[48] HOCl could trigger the oxidative hydrolysis of NHC boranes by hydride abstraction at the borane center to result in the formation of imidazolium salts (Scheme 1b). ESI-MS analysis of the reaction mixture of **4** (10 μM) with OCl^- (100 μM) was carried out to confirm this hypothesis. The molecular ion attributed to **4** disappeared, and was replaced by new a peak of m/z = 197 $[M]^+$, consistent with **3** (Figure S7).

The TPM images of **4**-labeled Raw 264.7 cells appeared to heterogeneously emit in the cells. To check the distribution of the probe at subcellular levels, colocalization experiments of **4** were conducted with endoplasmic reticulum (ER), mitochondria and lysosome commercial organelle trackers using Raw 264.7 cells (Figure 3). The cells were pretreated with 10 μM **4**, and then 1 μM ER-Tracker Red (or 1 μM Mito/Lyso-Tracker Red) for 30 min. The TPM image of **4** in Raw 264.7 cells showed considerable overlap with the one-photon microscopic (OPM) image of ER Tracker Red. By contrast, the distribution of **4** was weakly correlated with that of mitochondria and lysosome trackers. The Pearson's colocalization coefficient (A) value of 4 with ER tracker is 0.92, which is much higher than those with mito-tracker red (A = 0.59) and lyso-tracker red (A = 0.34). The result was confirmed by line profile analysis (Figure 3). Similar results were observed in colocalization experiments in HeLa and RKO cells between **4** and ER Tracker Red (Figure S10).

Generally, fluorescent sensors positioned in the ER region have 1) a cationic character, 2) a moderate size in conjugated band numbers (CBN < 40), and 3) an appropriate lipophilicity ($+6 > \log P_{oct} > 0$).[52] Probe **4** possess a cationic character bestowed by its imidazolium ring and a CBN of 16. The lipophilicity of **4**, determined by a partition experiment between PBS buffer (10 mM, pH 7.4) and 1-octanol, was found to be 1.04 ± 0.02 (Table S2), placing it in the proper range for accumulation in the ER.

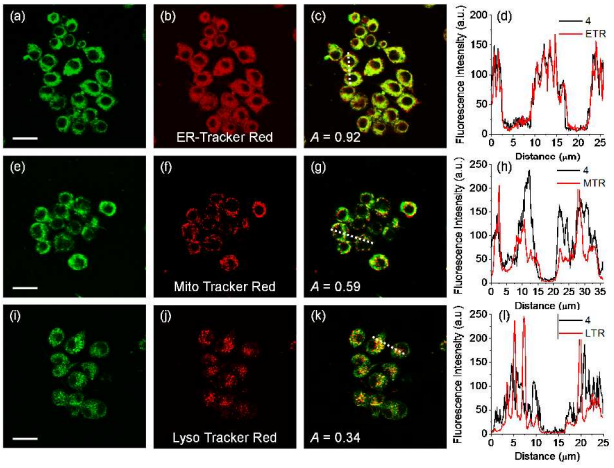

Figure 3. TPM (a, e and i), OPM (b, f and j) and merged (c, g and k) images of Raw 264.7 cells co-labeled with **4** (10 μM) and organelle trackers (1.0 μM). Line profile of fluorescence intensity (d, h and l) obtained from corresponding cells images. λ_{ex} for TPM and OPM are 720 nm and 552 nm, respectively, and the corresponding emissions were recorded at 380-550 nm (**4**) and 600-650 nm (organelle trackers). Scale bars = 20 μm.

Next, to confirm that **4** responds to OCl^- in living cells, the changes in average emission ratios (F_{green}/F_{blue}) of **4** following incubation with NaOCl in Raw 264.7 cells were examined. As the concentration of NaOCl increased (0-1 mM), the average intensity ratios (F_{green}/F_{blue}) of **4** increased from 3.2 to 6.3 (Figure S11). The applicability of **4** for sensing endogenous OCl^- in macrophages was then studied. Macrophages were stimulated by lipopolysaccharides (LPS) and interferon gamma (IFN-γ). H_2O_2 is produced and then converted into OCl^- by the myeloperoxidase enzyme (MPO) when the cells are treated with phorbol myristate acetate (PMA).[53] In Figure 4, the average emission ratio (F_{green}/F_{blue}) of **4** increased to 4.0 in Raw 264.7 cells pre-stimulated with LPS (100 ng mL^{-1}), IFN-γ (50 ng mL^{-1}) and PMA (10 nM). Treatment of the cells with the MPO inhibitors 4-aminobenzoic acid hydrazide (4-ABAH, 50 μM) or flufenamic acid (FFA, 50 μM) resulted in average intensity ratios (F_{green}/F_{blue}) undistinguishable from that of the control, confirming the specificity of the response (Figure 4e and f). Additionally, Raw 264.7 cells were incubated with inducers or antagonists of oxidative stress to further confirm that **4** selectively functions in the ER. Tunicamycin (Tm) is known to increase oxidative stress of the ER, increasing H_2O_2 generation; dithiothreitol (DTT), on the contrary, consumes H_2O_2 in the ER.[54] When cells were pretreated with Tm (10 μg mL^{-1}, Figure 4b), the average intensity ratio (F_{green}/F_{blue}) of **4** increased to its highest value, 5.8, whereas the average ratio decreased to 2.7 upon the addition of DTT (2 mM, Figure 4c). These outcomes reveal that 4 changes directly and mostly in response to OCl– levels in the ER of live cells, confirming its suitability for monitoring OCl^- by two-photon imaging microscopy.

Finally, the ability of **4** to detect OCl^- in fresh rat hippocampal slices was examined. In the hippocampal CA1 and CA3 regions, the average intensity ratios (F_{green}/F_{blue}) in the tissues incubated with **4** (100 μM) for 1.5 h were 3.3 and 3.1, respectively, values similar to those found in macrophages (Figure 5). By contrast, when hippocampal slices were pre-incubated with the stressor PMA (10 ng mL^{-1}) for 30 min, the average intensity ratios (F_{green}/F_{blue}) were increased to 3.7 in both the CA1 and CA3 regions.

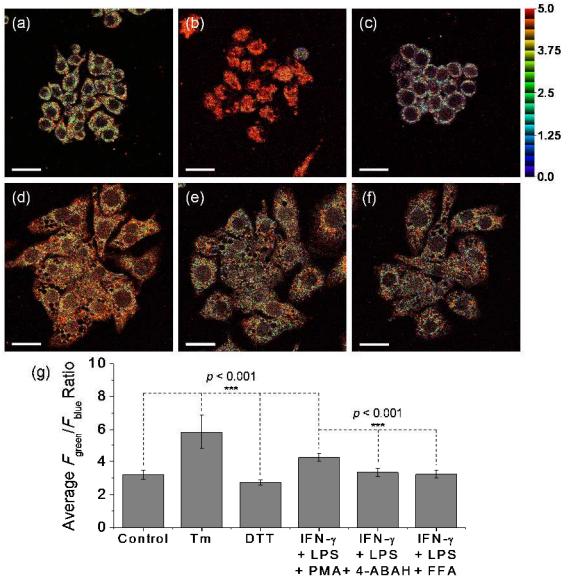

Figure 4. Pseudocolored ratiometric TPM images of Raw 264.7 cells labeled with **4** (10 μM) for 30 min. (a) Control image. Cells pretreated with (b) Tm (10 μg mL^{-1}, 16 h), (c) DTT (2 mM, 16 h), (d) LPS (100 ng mL^{-1}, 16 h), IFN-γ (50 ng mL^{-1}, 4 h) and PMA (10 nM, 30 min), (e) LPS, IFN-γ, PMA and 4-ABAH (50 μM, 4 h) and (f) LPS, IFN-γ, PMA and FFA (50 μM, 4h) and then treated with **4**. (g) Average ratios of F_{green}/F_{blue} in the TPM images. Asterisks indicate statistical significance (***) for $p < 0.001$.Excitation wavelength for **4** is 720 nm and TPM images were obtained at 450-600 nm (green) and 380-430 nm (blue). Scale bars = 20 μm.

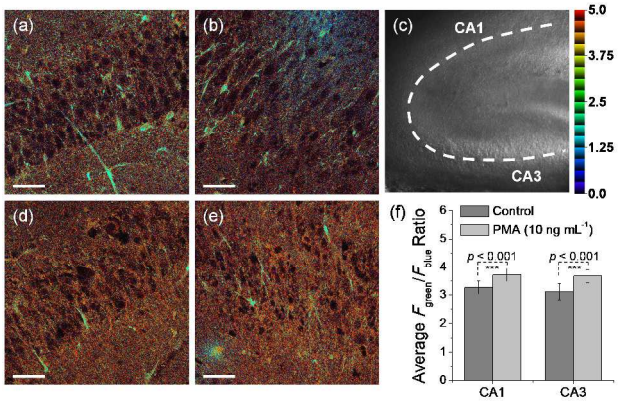

Figure 5. Pseudocolored ratiometric TPM images of rat hippocampal slices labeled with **4** (100 μM) for 1.5 h. TPM images of controls (a, b), and slices pre-treated with PMA (10 ng mL^{-1}, 30 min) (d, e), before loading with **4**. (c) Bright-field image of the CA1 and CA3 regions at the magnification of x10. (f) Average intensity F_{green}/F_{blue} ratios in the TPM images. Asterisks indicate statistical significance (***) for $p < 0.001$. Excitation wavelength for **4** was 720 nm, and the TPM images were obtained at 450-600 nm (green) and 380-430 nm (blue). Scale bars = 50 μm.

CONCLUSIONS

The fluorogenic naphthoimidazolium borane **4** was successfully developed into an ER-targeted probe for the ratiometric two-photon imaging of exogenous and endogenous HOCl in live cells and tissues. Upon oxidation of the B–H bonds by

HOCl and subsequent hydrolysis, it is converted to the emissive imidazolium salt **3**, giving rise to a turn-on response at 450 nm. The probe localizes in the ER, is highly selective for HOCl over other ROS, functions in a broad range of pH, and is less susceptible to aggregation effects than previously reported NHC-borane probes for HOCl, which relied on the modulation of pyrene excimer emission. These meritorious properties portend to the potential value of **4** in the study of ER signaling and function under oxidative stress.

ASSOCIATED CONTENT

Supporting Information

The Supporting Information is available free of charge on the ACS Publications website. Synthetic schemes and procedures, experimental details, ^{1}H NMR, ^{13}C NMR, ESI-MS, UV−Vis, and fluorescence spectra (Figures S1-S18; Tables S1-S2) (PDF).

AUTHOR INFORMATION

Corresponding Author

* E-mail: kimhm@ajou.ac.kr. Phone: +82 (031) 219-2609
* E-mail: bouffard@ewha.ac.kr. Phone: +82 (02) 3277-3427
* E-mail: jyoon@ewha.ac.kr. Phone: +82 (02) 3277-2400

ORCID

Hwan Myung Kim: 0000-0002-4112-9009
Jean Bouffard: 0000-0003-2281-2088
Juyoung Yoon: 0000-0002-1728-3970

Author Contributions

‡These authors contributed equally

Notes

The authors declare no competing financial interest.

ACKNOWLEDGMENT

We thank the National Research Foundation of Korea for the financial support (2012R1A3A2048814 to J. Y.; 2016R1E1A1A02920873 to H. M. K.; and 2018R1D1A1B07043568 to J. B). We also thank the Western Seoul (LC-MS) and Daegu (FAB) branches of the Korea Basic Science Institute for mass spectrometric data.

REFERENCES

1. Winterbourn, C. C. Reconciling the chemistry and biology of reactive oxygen species. *Nat. Chem. Biol*. **2008**, *4*, 278-286.
2. Breckwoldt, M. O.; Chen, J. W.; Stangenberg, L.; Aikawa, E. Rodriguez, E.; Qiu, S.; Moskowitz, M. A.; Weissleder, R. Tracking the inflammatory response in stroke in vivo by sensing the enzyme myeloperoxidase. *Proc. Natl. Acad. Sci. U. S. A*. **2008**, *105*, 18584-18589.
3. Barnham, K. J.; Masters, C. L.; Bush, A. I. Neurodegenerative diseases and oxidative stress. *Nat. Rev. Drug Discov*. **2004**, *3*, 205-214.
4. Finkel, T.; Serrano, M.; Blasco, M. A. The common biology of cancer and ageing. *Nature*. **2007**, *448*, 767-774.
5. Chen, X.; Wang, F.; Hyun, J.; Wei, T.; Qiang, J.; Ren, X.; Shin, I.; Yoon, J. Recent progress in the development of fluorescent, luminescent and colorimetric probes for detection of reactive oxygen and nitrogen species. *Chem. Soc. Rev*. **2016**, *45*, 2976-3016
6. Chen, X.; Tian, X.; Shin, I.; Yoon, J. Fluorescent and luminescent probes for detection of reactive oxygen and nitrogen species. *Chem. Soc. Rev*. **2011**, *40*, 4783-4804
7. Ren, M.; Zhou, K.; He, L.; Lin, W. Mitochondria and lysosome-targetable fluorescent probes for HOCl: recent advance and perspectives. *J. Mater. Chem. B*. **2018**, *6*, 1716-1733
8. Andina, D.; Leroux, J. C.; Luciani, P. Ratiometric Fluorescent Probes for the Detection of Reactive Oxygen Species. *Chem. Eur. J*. **2017**, *23*, 13549-13573
9. Lou, Z.; Li, P.; Han, K. Redox-Responsive Fluorescent Probes with Different Design Strategies. *Acc. Chem. Res*. **2015**, *48*, 1358-1368
10. Hu, J. J.; Wong, N. K.; Gu, Q.; Bai, X.; Ye, S.; Yang, D. HKOCl-2 Series of Green BODIPY-Based Fluorescent Probes for Hypochlorous Acid Detection and Imaging in Live Cells. *Org. Lett*. **2014**, *16,* 3544-3547
11. Yuan, L.; Wang, L.; Agrawalla, B. K.; Park, S. J.; Zhu, H.; Sivaraman, B.; Peng, J.; Xu, Q. H.; Chang, Y. T. Development of Targetable Two-Photon Fluorescent Probes to Image Hypochlorous Acid in Mitochondria and Lysosome in Live Cell and Inflamed Mouse Model. *J. Am. Chem. Soc*. **2015**, *137*, 5930-5938.
12. Chen, X.; Lee, K.-A.; Ren, X.; Ryu, J.-C.; Kim, G.; Ryu, J.-H.; Lee, W.-J.; Yoon, J. Synthesis of highly HOCl-selective fluorescent probe and its use for imaging HOCl in cells and organisms. *Nat. Protocols*. **2016**, *11*, 1219-1228.
13. Chen, S.; Lu, J.; Sun, C.; Ma, H. A highly specific ferrocene-based fluorescent probe for hypochlorous acid and its application to cell imaging. *Analyst*. **2010**, 135, 577-582.
14. Kenmoku, S.; Urano, Y.; Kojima, H.; Nagano, T. Development of a Highly Specific Rhodamine-Based Fluorescence Probe for Hypochlorous Acid and Its Application to Real-Time Imaging of Phagocytosis. *J. Am. Chem. Soc*. **2007**, *129*, 7313-7318.
15. Chen, G.; Song, F.; Wang, J.; Yang, Z.; Sun, S.; Fan, J.; Qiang, X.; Wang, X.; Dou, B.; Peng, X. FRET spectral unmixing: a ratiometric fluorescent nanoprobe for hypochlorite. *Chem. Commun.* **2012**, *48*, 2949-2951.
16. Wang, B.; Chen, D.; Kambam, S.; Wang, F.; Wang, Y.; Zhang, W.; Yin, J.; Chen, H.; Chen, X. A highly specific fluorescent probe for hypochlorite based on fluorescein derivative and its endogenous imaging in living cells. *Dyes Pigments*. **2015***, 120***,** 22-29.
17. Srikun, D.; Miller, E. W.; Domaille, D. W.; Chang, C. J. An ICT-Based Approach to Ratiometric Fluorescence Imaging of Hydrogen Peroxide Produced in Living Cells. *J. Am. Chem. Soc*. **2008**, *130*, 4596-4597.
18. Lou, Z.; Li, P.; Panab, Q.; Han, K. A reversible fluorescent probe for detecting hypochloric acid in living cells and animals: utilizing a novel strategy for effectively modulating the fluorescence of selenide and selenoxide. *Chem. Commun*., **2013**, *49*, 2445-2447.
19. Zhang, W.; Liu, W.; Li, P.; Kang, J.; Wang, J.; Wang, H.; Tang, B. Reversible two-photon fluorescent probe for imaging of hypochlous acid in live cells and in vivo. *Chem. Commun*., **2015**, *51*, 10150-10153.
20. Li, P.; Zhang, W.; Li, K.; Liu, X.; Xiao, H.; Zhang, W.; Tang, B. Mitochondria-targeted reaction-based two-photon fluorescent probe for imaging of superoxide anion in live cells and in vivo. *Anal. Chem*. **2013**, *85*, 9877-9881
21. Xu, W.; Zeng, Z.; Jiang, J-H.; Chang, Y-T.; Yuan, L. Discerning the Chemistry in Individual organelles with Small-Molecule Fluorescent Proves. *Angew. Chem. Int. Ed*. **2016**, *55*, 13658-13699.
22. Zhu, H.; Fan, J.; Du, J.; Peng, X. Fluorescent Probes for Sensing and Imaging within Specific Cellular Organelles. *Acc. Chem. Res*. **2016**, *49*, 2115-2126.
23. Satori, C. P.; Henderson, M. M.; Krautkramer, E. A.; Kostal, V.; Distefano, M. M.; Arriaga, E. A. Bioanalysis of Eukaryotic Organelles. *Chem. Rev*. **2013**, *113*, 2733-2811.
24. Zielonka, J.; Joseph, J.; Sikora, A.; Hardy, M.; Ouari, O.; Vasquez-Vivar, J.; Cheng, G.; Lopez, M.; Kalyanaraman, B. Mitochondria-Targeted Triphenylphosphonium-Based Compounds: Syntheses, Mechanisms of Action, and Therapeutic and Diagnostic Applications. *Chem. Rev*. **2017**, *117*, 10043-10120.
25. Ron, D.; Walter, P. Signal integration in the endoplasmic reticulum unfolded protein response. *Nature Reviews Molecular Cell Biology*. **2007**, *8*, 516-529.

26. Mandl, J.; Meszaros, T.; Banhegyi, G.; Hunyady, L.; Csala, M. Endoplasmic reticulum: nutrient sensor in physiology and pathology. *Trends Endocrinol. Metab.* **2009**, *20*, 194-201.
27. Gao, C.; Tian, Y.; Zhang, R.; Jing, J.; Zhang, X. Endoplasmic Reticulum-Directed Ratiometric Fluorescent Probe for Quantitive Detection of Basal H2O2. *Anal. Chem*. **2017**, *89*, 12945-12950.
28. Schröder, M.; Kaufman, R. J. THE MAMMALIAN UNFOLDED PROTEIN RESPONSE. *Annual Review Biochemistry*. **2005**, *75*, 739-789.
29. Tu, B. P.; Weissman, J. S. Oxidative protein folding in eukaryotes: mechanisms and consequences. *J. Cell Biol*. **2004**, *164*, 341-346.
30. Shimizu, Y.; Hendershot, l. M. Oxidative Folding: Cellular Strategies for Dealing with the Resultant Equimolar Production of Reactive Oxygen Species. *Antioxidants & Redox Signalling*. **2009**, *11*, 2317-2331.
31. Dickinson, B. C.; Chang, C. J. Chemistry and biology of reactive oxygen species in signaling or stress responses. *Nat Chem Biol.* **2011**, *7*, 504-511.
32. Guo, Z.; Shin, I.; Yoon, J. Recognition and sensing of various species using boronic acid derivatives. *Chem. Commun.* **2012**, *48*, 5956-5967.
33. Zielonka, J.; Sikora, A.; Hardy, M.; Joseph, J., Dranka, B. P.; Kalyanaraman, B. Boronate Probes as Diagnostic Tools for Real Time Monitoring of Peroxynitrite and Hydroperoxides. *Chem Res Toxicol*. **2012**. *25*, 1793-1799.
34. Lo, L.-C.; Chu, C.-Y. Developement of highly seletive and sensitive probes for hydrogen peroxide. *Chem. Commun*. **2003**, 2728-2729.
35. Chang, M.; Pralle, A.; Isacoff, E. Y.; Chang, C. J. A Selective, Cell-Permeable Optical Probe for Hydrogen Peroxide in Living Cells. *J. Am. Chem. Soc.* **2004**, *126*, 15392-15393.
36. Miller, E. W.; Albers, A. E.; Pralle, A.; Isacoff, E. Y.; Chang, C. J. Boronate-Based Fluorescent Probes for Imaging Cellular Hydrogen Peroxide. *J. Am. Chem. Soc*. **2005**, *127*, 16652-16659.
37. Karton-Lifshin, N.; Segal, E.; Omer, L.; Portnoy, M.; Satchi-Fainaro, R.; Shabat, D. A Unique Pradigm for a Turn-ON Near-Infrared Cyanine-Based Probe: Noninvasive Intravital Optical Imaging of Hydrogen Peroxide. *J. Am. Chem. Soc.* **2011**, *133*, 10960-10965.
38. Du, L.; Li, M.; Zheng, S.; Wang, B. Rational Design of a Fluorescent Hydrogen Peroxide Probe Based on Umbelliferone Fluorophore. *Tetrahedron Lett.* **2008**, *49*, 3045-3048.
39. Michalski, R.; Zielonka, J.; Gapys, E.; Marcinek, A.; Joseph, J.; Kalyanaraman, B. Real-time Measurements of Amino Acid and Protein Hydroperoxides Using Coumarin Boronic Acid. *J. Biol. Chem.* **2014**, *289*, 22536-22553.
40. Hanna, R. D.; Naro, Y.; Dieters, A.; Floreancig, P. E. Alcohol, Aldehyde, and Ketone Liberation and Intracellular Cargo Release through Peroxide-Mediated α-Boryl Ether Fragmentation. *J. Am. Chem. Soc.* **2016**, *138*, 13353-13360.
41. Li, H.; Yao, Q.; Fan, J.; Du, J.; Wang, J.; Peng, X. A two-photon NIR-to-NIR fluorescent probe for imaging hydrogen peroxide in living cells. *Biosens. Bioelectron.* **2017**, *94*, 536-543.
42. Xu, Q.; Lee, K.-A.; Lee, S.; Lee, K. M.; Lee, W.-J.; Yoon, J. A Highly Specific Fluorescent Probe for Hypochlorous Acid and Its Application in Imaging Microbe-Induced HOCl Production. *J. Am. Chem. Soc*. **2013**, *135*, 9944-9949.
43. Wang, Q.; Liu, C.; Chang, J.; Lu, Y.; He, S.; Zhao, L.; Zeng, X. Novel water soluble styrylquinolinium boronic acid as a ratiometric reagent for the rapid detection of hypochlorite ion. *Dyes and Pig.* **2013**, *99*, 733-739.
44. Sikora, J. Zielonka, M. Lopez, J. Joseph, Kalyanaraman, B. Direct oxidation of boronates by peroxynitrite : mechanism and implications in fluorescence imaging of peroxynitrite. *Free Rad. Biol. Med.* **2009**, *47*, 1401-1407;
45. Zielonka, J.; Sikora, A.; Joseph, J.; Kalyanaraman, B. Peroxynitrite is the major species formed from different flux ratios of co-generated nitiric oxide and superoxide : direct reason with boronate-based fluorescent probe. *J. Biol. Chem.* **2010**, *285*, 14210-14216.
46. Yu, F.; Song, P.; Li, P.; Wang, B.; Han, K. A fluorescent probe directly detect peroxynitrite based on boronate oxidation and its applications for fluorescence imaging in living cells. *Analyst.* **2012**, *137*, 3740-3749.
47. Sun, Z.; Xu, Q.; Kim, G.; Flower, S. E.; Lowe, J. P.; Yoon, J.; Fossey, J. S.; Qian, X.; Bull, S. D.; James, T. D. A water-soluble boronate-based fluorescent probe for the selective detection of peroxinitrite and imaging in living cells. *Chem. Sci.* **2014**, *5*, 3368-3373.
48. Pak, Y. L.; Park, S. J.; Wu, D.; Cheon, B.; Kim, H. W.; Bouffard. J.; Yoon, J. N-Heterocyclic Carbene Boranes as Reactive Oxygen Species-Responsive Materials: Application to the Two-Photon Imaging of Hypochlorous Acid in Living Cells and Tissues. *Angew. Chem. Int. Ed*. **2018**, *57*, 1567-1571.
49. Xu, Q.; Heo, C. H.; Kim, G.; Lee, H. W.; Kim, H. M.; Yoon, J. Development of imidazoline-2-thiones based two-photon fluorescence probes for imaging hypochlorite generation in a co-culture system. *Angew. Chem. Int. Ed*. **2015**, *54*, 4890-4894.
50. Güçlü, K.; Kibrislioglu, G.; Özyürek, M.; Apak, M. Development of a Fluorescent Probe for Measurement of Peroxyl Radical Scavenging Activity in Biological Samples. *J. Agric. Food Chem.*, **2014**, *62*, 1839-1845.
51. Halliwell. P, Evans. M, Whiteman. Assessment of peroxynitrite scavengers in vitro. *Methods in Enzymology*. **1999**, *301*, 333-342.
52. Colston, J.; Horobin, R, Rashid-Doubell, F.; Pediani, J.; Johal, K. K. Why fluorescent probes for endoplasmic reticulum are selective: an experimental and QSAR-modelling study. *Biotech. Histochem.*, **2003**, *78*, 323-332.
53. Spalteholz, H.; Panasenko, O. M.; Arnhold, J. Formation of reactive halide species by myeloperoxidase and eosinophil peroxidase. *Arch. Biochem. Biophys.* **2006**, *445*, 225-234.
54. Wu, R.-F.; Ma, Z.; Liu, Z.; Terada, L. S. Nox4-derived H2O2 mediates endoplasmic reticulum signaling through local Ras activation. *Mol. Cell. Biol.* **2010**, *30*, 3553-3568.

TOC